Photoconductivity in donor-acceptor heterojunction organic photovoltaics

C. K. Renshaw,[1] J. D. Zimmerman,[2] B. E. Lassiter,[3] and S. R. Forrest[1,2,3]
[1]*Department of Physics, University of Michigan, Ann Arbor, Michigan 48109, USA*
[2]*Department of Electrical Engineering and Computer Science, University of Michigan, Ann Arbor, Michigan 48109, USA*
[3]*Department of Materials Science and Engineering, University of Michigan, Ann Arbor, Michigan 48109, USA*
(Received 15 April 2012; revised manuscript received 24 July 2012; published 27 August 2012)

Organic photovoltaics (OPVs) differ from ideal inorganic solar cells due to their pronounced voltage dependence under reverse bias. This feature is commonly modeled in an *ad hoc* fashion by including a parallel junction resistance (R_p) that bypasses the heterojunction energy barrier between donor and acceptor. The existence of a finite R_p has variously been attributed to rough interfaces, pinhole defects, or to the electric field dependence of the dissociation of polaron pairs that are bound at the heterojunction. Here we show that the voltage dependence of the photocurrent can also arise from photoconductivity resulting from exciton generation followed by dissociation into free polarons within the bulk of the donor and acceptor layers. The presence of photoconductivity of the active layers does not result in an increase in power conversion efficiency, and places a constraint on the maximum fill factor that can be achieved in an OPV cell.

DOI: 10.1103/PhysRevB.86.085324 PACS number(s): 81.05.Fb, 88.40.jr, 71.35.−y

I. INTRODUCTION

Organic photovoltaic (OPV) cells have been demonstrated with power conversion efficiencies (η) approaching 10%.[1,2] To reach a high η, considerable effort has been invested to select materials and device architectures that maximize the OPV open-circuit voltage (V_{oc}), short-circuit current density (J_{sc}), and fill factor (FF). Factors that lead to high V_{oc} and J_{sc} are readily understood in terms of the offset of the frontier orbital energies of the donor and acceptor materials, optical absorption, exciton diffusion length, and the recombination dynamics of photogenerated charges within the cell.[3,4] However, the underlying physical processes and materials characteristics that result in a high FF are less well understood. This parameter is frequently treated using an equivalent circuit model for the current density vs voltage (J-V) characteristics, as shown in Fig. 1(a). The model may include a second, reverse-biased diode[5,6] to account for an "S-kink," and a parallel (i.e., shunt) resistance[7–9] (R_p) to account for a linear increase of photocurrent with reverse bias. The effect of R_p on the J-V characteristic, and particularly on FF, is shown in the inset [Fig. 1(a)].

Many physical models for the voltage dependence of FF consider the electric field dependence of the dissociation of polaron pairs (PPs) Coulombically bound at the interface. The dynamics of this dissociation process have been described by Onsager[10] and Braun.[11] Subsequently, numerous studies have applied this theory to analyze the voltage dependence of photocurrent in OPVs.[12–16] Recently, Giebink *et al.*[17] developed an analytical formalism describing the J-V characteristics of OPVs using a model based on the dynamics of free polarons and polaron pairs (PPs). This model provides a physical framework for many common features of the OPV J-V characteristics, including the double exponential character of the forward-biased dark current, the heterojunction ideality factor (n), the "S-kink" behavior, and the voltage dependence of the photocurrent (J_{ph}) which leads to a reduced FF. In that model, J_{ph} varies with voltage due to the electric field (F) induced polaron-pair dissociation rate (k_{PPd}), which can be described by the Onsager-Braun (O-B)[10,11] theory for Coulombically interacting charge pairs in a dielectric medium:

$$k_{PPd} = \frac{3}{4\pi a^3} k_{rec} \exp(-E_B/k_B T)[J_1(2\sqrt{-2b})/\sqrt{-2b}]. \quad (1)$$

Here a is the initial PP separation at the heterointerface, k_{rec} is the Langevin rate for free polarons to form PPs, E_B is the PP binding energy and is approximated by $E_B = q^2/4\pi\varepsilon a$, J_1 is the first order Bessel function of the first kind, $b = -q^3 F_I/(8\pi\varepsilon k_B{}^2 T^2)$, and F_I is the interface electric field. Also, q is the electronic charge, ε is the material permittivity, k_B is Boltzmann's constant, and T is the temperature. The dissociation leads to a sublinear increase in J_{ph} under reverse bias according to $J_{ph} = J_{jxn} = \eta q J_X$, where J_{jxn} is the photocurrent produced at the donor-acceptor heterojunction (D-A HJ), $\eta = k_{PPd}/(k_{PPd} + k_{PPr})$ is the PP dissociation efficiency, k_{PPr} is the PP recombination rate, and J_X is the exciton flux reaching the HJ that produces PPs. It has been proposed that the field dependence of k_{PPd} is the underlying physical process that results in a finite R_p commonly observed in OPVs.[17]

Here we show that the observed linear dependence of J_{ph} on voltage can be quantitatively explained by photoconductivity due to exciton generation followed by dissociation in the donor and acceptor bulks, as also identified by Jeong *et al.*[18] This is a significant effect common to many OPVs that often masks the underlying, intrinsic field-dependent dissociation of PPs at the heterojunction.[17,19] In this study we treat the simple case of planar heterojunction OPVs; however photoconductivity is an intrinsic process in all semiconductors. Hence, it is expected to be present even in other OPV device architectures such as bulk heterojunctions (BHJs). In the latter case, PP dissociation depends on the microscopic orientation of D/A domains, and charge collection is strongly affected by bimolecular recombination throughout the bulk, which can lead to a more complicated analysis than in simple planar morphologies. We note, however, that whether or not photoconductivity plays a dominant role compared with other processes such as field-dependent dissociation or bimolecular charge recombination,

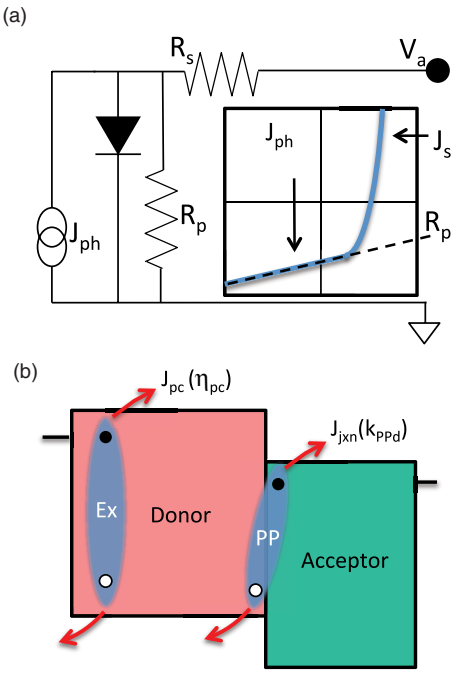

FIG. 1. (Color online) (a) Equivalent circuit and (inset) the characteristic shape of the current-density vs voltage (J-V) characteristic for a heterojunction (HJ) organic photovoltaic (OPV) device. The parallel resistance (R_p) is due to photoconductivity and results in a linear slope under reverse bias. (b) Schematic of the OPV device consisting of a donor and acceptor junction. At the HJ, excitons can split into polaron pairs (PPs) that are dissociated at a rate $k_{\rm PPd}$ to generate photocurrent from the junction ($J_{\rm jxn}$). Photogenerated excitons can also result in free carriers in the bulk of the organic films with a photoconductive efficiency, $\eta_{\rm pc}$, and contribute a current due to photoconductivity ($J_{\rm pc}$) to the total photocurrent.

depends on the details of the junction morphology in each case. These considerations will be discussed in Sec. IV.

II. THEORY

In excitonic materials where Coulomb interactions between electrons and holes are much larger than the thermal energy, photon absorption generates a bound exciton state that, on dissociation, contributes to the current. Dissociation can be efficient at a D-A HJ when there is an energy offset sufficient to separate the electron and hole[19] into the acceptor and donor layers, respectively. After charge transfer, Coulomb attraction results in a bound PP state at the interface [see Fig. 1(b)]. In this case, the current is determined exclusively by PP kinetics at the interface that are described using

$$J = J_{sD}\left\{\exp\left[\frac{q(V_a - JR_s)}{n_D k_B T}\right] - \frac{k_{\rm PPd}}{k_{\rm PPd,eq}}\right\} + J_{sA}\left\{\exp\left[\frac{q(V_a - JR_s)}{n_A k_B T}\right] - \frac{k_{\rm PPd}}{k_{\rm PPd,eq}}\right\} - J_{\rm jxn}. \quad (2)$$

Here J_{sD}, J_{sA}, n_D, and n_A are the saturation current densities and ideality factors defined in Ref. 17, V_a is the applied voltage, R_s is the series resistance, and $k_{\rm PPd,eq} = k_{\rm PPd}(V_a = 0)$ is the equilibrium dissociation rate. Equation (2) assumes a separation distance a between electron and hole polarons

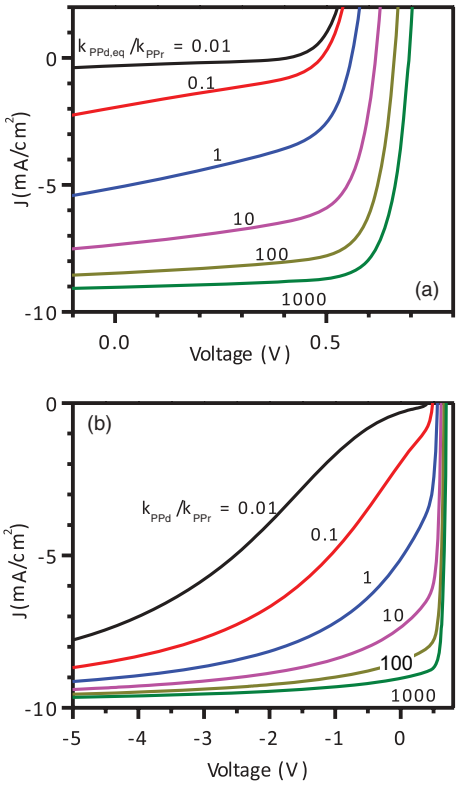

FIG. 2. (Color online) (a) Calculated current-density vs voltage (J-V) characteristics for an organic solar cell according to Eq. (2) in text, with various ratios of the equilibrium polaron pair (PP) dissociation to the recombination rate ($k_{\rm PPd,eq}/k_{\rm PPr}$). (b) The same calculation as in (a) extended to larger reverse bias to emphasize the nonlinear behavior of the O-B process.

across the interface. To account for the effects of interface disorder, we average over a normal distribution of initial D-A molecular separations using

$$\langle J\rangle = \int_0^\infty \frac{4}{\sqrt{\pi}a_0^3} a^2 \exp\left(-\frac{a^2}{a_0^2}\right) J(a)da. \quad (3)$$

Here a_0 is the characteristic initial PP separation.[19] In Fig. 2 we calculate the current for various values of $k_{\rm PPr}$ from Eq. (1) and using the parameters defined in Table I. Note that it is the *ratio* $k_{\rm PPd,eq}/k_{\rm PPr}$ that determines the dependence of $J_{\rm jxn}$ on V_a (cf. Fig. 7 in Ref. 17 where $k_{\rm PPd,eq}^{-1} = 140$ ns was assumed), and hence the fill factor of the OPV. For this calculation we assume $a_0 = 2$ nm and $V_a = 0$ V. Also, when the applied voltage is greater than the built-in potential (i.e. $V_a > V_{bi}$), Eq. (1) is no longer valid. Hence, we use the zero-field value $k_{\rm PPd}(V_{bi})$ for the PP dissociation rate, but add $\delta E = qF_I(\sqrt{r_c^2 - a^2\sin^2\theta} - a\cos\theta)$ to the binding energy to account for the additional energy needed to separate charge normal to the interface when $F_I > 0$. Here θ is the angle of the PP separation vector relative to the interface normal, $r_C = q^2/4\pi\varepsilon k_B T$ is the Onsager exciton radius,[20] and we average over the half-space, $-\pi/2 < \theta < \pi/2$, of possible PP orientations. With $\varepsilon/\varepsilon_0 = 3$ as in Table I, $r_c \approx 18$ nm $\gg a_0$ and $\delta E \approx qF_I r_C$.

Figure 2 shows that the shape of the J-V characteristics and the resulting FF are strongly dependent on the recombination

TABLE I. Model parameter values.

Parameter	Value[a]	Definition
d	80 nm	Total thickness of the organic layers
ΔE_{HL}	1.2 eV	Interfacial energy gap
V_{bi}	0.8 V	Built-in voltage
$T_{t,A} = T_{t,D}$	1000 K	Characteristic temperature for hole and electron trap distributions in the donor and acceptor
$H_A = H_D$	10^{18} cm^{-3}	Trap densities in the donor and acceptor
$N_{\mathrm{HOMO}} = N_{\mathrm{LUMO}}$	10^{21} cm^{-3}	Band-edge density of states of the HOMO (donor) and LUMO (acceptor)
δ_A	0.5	Fraction of voltage dropped across the acceptor
a_0	2 nm	Characteristic polaron pair separation
$k_{\mathrm{rec,n}} = k_{\mathrm{rec,p}} = q\mu/\varepsilon$	$\varepsilon/\varepsilon_0 = 3$, $\mu = 10^{-3}$ cm^2/Vs	Free carrier bimolecular recombination rate
R_s	1 Ωcm^2	External series resistance
S_{pc}	0.9 mA/Vcm^2	Photoconductance
$\phi_{\mathrm{anode}} = \phi_{\mathrm{cathode}}$	0.2 eV	Injection barrier at the cathode and anode

[a]Model values based on Ref. 17.

rate. In the fourth quadrant [Fig. 2(a)] a linear dependence of J_{ph} on V_a was found with the magnitude of the slope dependent on $k_{\mathrm{PPd,eq}}/k_{\mathrm{PPr}}$. Under these conditions, when $1 < k_{\mathrm{PPd,eq}}/k_{\mathrm{PPr}} < 100$, the calculated J-V characteristics following Eq. (2) are found to be typical of conventional, planar OPVs. Indeed, this effect has often been explained[7,8] using a parallel resistance (R_p) that serves as a proxy for the underlying physics described by PP dissociation. At higher reverse bias there is a significant departure from linearity except in the case of very high PP dissociation rates in O-B dominated processes, as shown in Fig. 2(b).

In Fig. 3(a) we show that the current deviates from a linear dependence on voltage if, in fact, k_{PPd} is determined only by O-B dissociation, as assumed for the analysis in Ref. 17. Additionally, we expect a pronounced temperature dependence in the J-V characteristics since PP dissociation is a thermally activated process, as also shown in Fig. 3(a). In practice, however, OPVs often exhibit a photocurrent J_{ph} that is linearly dependent on V_a over a large voltage and temperature range, indicating that Onsager-Braun dissociation inadequately describes the observed reverse J-V characteristics.

To explain the linear reverse-biased characteristics, we include the effect of direct carrier generation from excitons in the organic semiconductor bulk layers[20,21] by, for example, exciton-assisted polaron detrapping,[22] field-induced barrier lowering,[23] or thermally induced exciton dissociation.[24] Generation of carriers in the bulk can also increase the electron and hole densities, viz., $n = n_0 + n_{\mathrm{pc}}$ and $p = p_0 + p_{\mathrm{pc}}$, where n_0 (p_0) is the electron (hole) density in the dark, and n_{pc} (p_{pc}) is the additional photogenerated electron (hole) density. The photocurrent is

$$J_{\mathrm{pc}} = q(n_{\mathrm{pc}}\mu_e + p_{\mathrm{pc}}\mu_h)F, \tag{4}$$

where F is the electric field across the layers, and μ_e (μ_h) is the electron (hole) mobility. For sufficiently small carrier densities, Ohmic conduction dominates, in which case the electric field is $F = (V_a - V_{bi})/d$, where the voltage drops across the small internal layer and contact resistances have been ignored. Here V_{bi} is equal to the offset in anode and cathode contact work functions, and d is the sum of the donor- and acceptor-layer thicknesses. This approximation is valid when the applied voltage is more than 0.1 V below V_{bi}, where numerical simulations of the complete device by self-consistently solving the drift-diffusion equations (including PP generation and dissociation into free carriers) indicate that the electric field varies by less than 10% throughout the device. The equilibrium photogenerated electron density is given by $n_{\mathrm{pc}} = \eta_{\mathrm{pc}} G\tau_e$, with a similar expression for holes. Here G is the exciton generation rate per unit volume, η_{pc} is the photoconductive efficiency given by the fraction of excitons that dissociate into free carriers in the bulk, and τ_e (τ_h) is the smaller of the electron (hole) lifetime or transit time. This yields a current of

$$J_{\mathrm{pc}} = e\eta_{\mathrm{pc}} G(\tau_e\mu_e + \tau_h\mu_h)(V_a - V_{bi})/d = S_{\mathrm{pc}}(V_a - V_{bi}), \tag{5}$$

where S_{pc} is the effective photoconductance.

Photoconductivity is a linear process that can result in a corresponding linear slope in the J-V characteristic under reverse bias. That is, referring to Fig. 1(a), we infer that $R_p = 1/S_{\mathrm{pc}}$ when photoconductivity dominates over field-induced PP dissociation [cf. Eq. (1)]. Photocarrier generation is added to the total photocurrent $J_{\mathrm{ph}} = J_{\mathrm{jxn}} + J_{\mathrm{pc}}$, yielding a modified ideal diode equation:

$$\begin{aligned} J = {} & J_{sD}\left(\exp\left(\frac{q(V_a - JR_s)}{n_D k_B T}\right) - \frac{k_{\mathrm{PPd}}}{k_{\mathrm{PPd,eq}}}\right) \\ & + J_{sA}\left\{\exp\left[\frac{q(V_a - JR_s)}{n_A k_B T}\right] - \frac{k_{\mathrm{PPd}}}{k_{\mathrm{PPd,eq}}}\right\} \\ & - J_{\mathrm{jxn}} + S_{\mathrm{pc}}(V_a - JR_s - V_{bi}). \end{aligned} \tag{6}$$

In Fig. 3(a) we plot J vs V according to Eq. (6), with $S_{\mathrm{pc}} = 0.9$ mA/Vcm^2 for both $k_{\mathrm{PPd,eq}}/k_{\mathrm{PPr}} = 0.7$ and 7000. Omitting the effects of photoconductivity, k_{PPr} is overestimated to fit the voltage dependence of J_{ph}. Figures 2 and 3(a) show that J_{jxn} has a nonlinear voltage dependence consistent with the O-B process. In contrast, J_{ph} is linear, as consistent with its photoconductive origin. Including photoconductivity results in a reduced estimate for k_{PPr} inferred from the fourth quadrant J-V characteristics, leading to a saturation in J_{jxn} even at low fields [open circles, Fig. 3(a)].

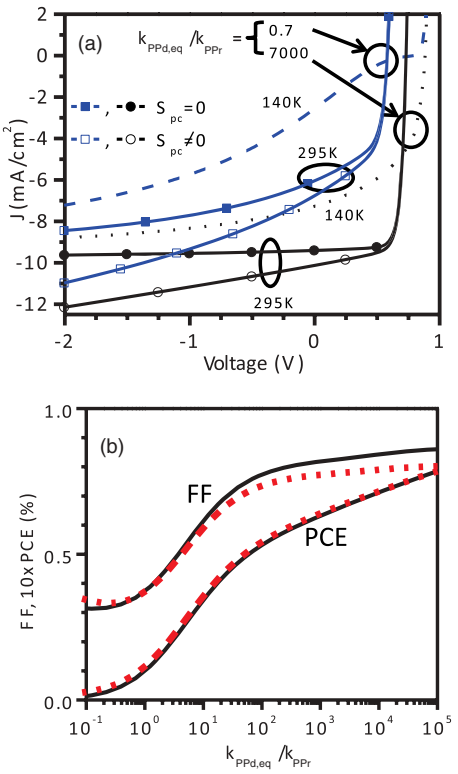

FIG. 3. (Color online) (a) Calculated current-density vs voltage (J-V) characteristics for an organic photovoltaic cell according to Eq. (2) in text, with the ratio of polaron pair (PP) dissociation rate to the PP recombination rate $k_{PPd,eq}/k_{PPr} = 7000$ (filled circles) and 0.7 (filled squares) at temperature $T = 295$ K. The same calculation is provided for $T = 140$ K for $k_{PPd,eq}/k_{PPr} = 7000$ (dotted line) and 0.7 (dashed line). The effect of photoconductivity is shown according to Eq. (6) in text, with $S_{pc} = 0.9$ mA/Vcm^2 for $k_{PPd,eq}/k_{PPr} = 7000$ (open circles) and 0.7 (open squares). (b) The dependence of the fill factor and power conversion efficiency on $k_{PPd,eq}/k_{PPr}$, including (dashed lines) and excluding (solid line) the effects of photoconductivity.

In Fig. 3(b) we calculate FF and power conversion efficiency (PCE) as functions of $k_{PPd,eq}/k_{PPr}$, both including (dashed) and excluding (solid) the effects of photoconductive charge generation in the layer bulks. In both cases, FF saturates for $k_{PPd,eq}/k_{PPr} > 100$ due to efficient PP dissociation and saturation of J_{jxn}. The reduced FF in the presence of photoconductivity is due to the increased J_{sc}; however PCE is not affected since J_{pc} is negligible at the OPV maximum power point (i.e., $MPPT = J_m$ V$_m$, where J_m is the current density at $MPPT$) of operation.

III. EXPERIMENT

Organic photovoltaic devices were fabricated on 1500-Å-thick indium tin oxide (ITO) films patterned into 1-mm-wide stripes on a glass substrate. The ITO surface was prepared by solvent cleaning, followed by 10 min exposure to UV-ozone to lower its work function.[25] Prior to use, donor and acceptor source materials were purified once by vacuum thermal-gradient sublimation. The substrate was loaded into a high vacuum thermal evaporator (base pressure $<2 \times 10^{-7}$ Torr) to deposit the organic layers. Following organic layer deposition, the cathode was patterned by deposition of Ag through a shadow mask with 1-mm-wide stripes, and positioned on the film surface inside a glove box filled with ultrahigh purity N_2 to prevent exposure to air during sample preparation. Devices were fabricated with the structure: ITO/boron subphthalocyanine chloride (SubPc) (130 Å)/C_{60} (400 Å)/bathocuproine (BCP) (80 Å)/Ag (1000 Å). A planar device architecture was chosen for this study because it offers a simple geometry for modeling the device. Here BCP was employed as an exciton blocking layer and optical spacer to improve device efficiency. Layer thicknesses were chosen to yield high efficiency devices. Devices were characterized at various light intensities using illumination from a solar simulator filtered to approximate an AM1.5G spectrum. The temperature-dependent J-V characteristics in the dark and under illumination were obtained using a liquid N_2 cryostat and a 1000 W Oriel solar simulator.

Single layer, photoconductor devices were similarly fabricated, but with the structure: ITO (1500 Å)/SubPc (600 Å)/Ag (1000 Å) and ITO (1500 Å)/C60 (600 Å)/Ag (1000 Å). This architecture was chosen to remove the D/A HJ and enable the direct measurement of photocurrent generated in the bulk of the organic films. The organic layer thickness was chosen to be similar to that used in the OPV devices. Synchronous measurements using a lock-in amplifier in conjunction with incident light from a 100 mW/cm^2 solar simulator, an argon laser at a wavelength of $\lambda = 514$ nm, and a diode laser at $\lambda = 409$ nm chopped at 200 Hz were used for voltage-dependent photocurrent measurements. Speed of response measurements were performed using a 1 ns pulse width, 5 nJ pulsed nitrogen laser at $\lambda = 337$ nm.

IV. RESULTS

Figure 4 shows the J-V characteristics of a SubPc/C_{60} OPV as a function of illumination intensity. There is a linear response of J_{ph} with voltage at $V_a < 0.5$ V. The photocurrent vs light intensity has a slope of $m = 15.7 \pm 0.6$ μA/mWV and intercept of $S_{pc,0} = 0.6 \pm 0.5$ μA/Vcm^2 (inset, Fig. 4). Figure 4(b) shows the linear behavior of the illuminated J-V characteristic over a large range of reverse bias. The maximum reverse voltage applied is limited by dielectric breakdown of the organic layers. Figure 5 shows the J-V characteristics at 1-sun illumination as a function of temperature. Here S_{pc} has a weak temperature dependence; at 100 mW/cm^2 it decreases from 1.25 ± 0.01 mA/Vcm^2 at $T = 300$ K, and saturates to 1.11 ± 0.01 mA/Vcm^2 at 217 K. We also studied photoconductor devices to quantitatively understand the origin and magnitude of S_{pc}. Figure 6 shows the voltage and light intensity-dependent photocurrent for an ITO/SubPc/Ag photoconductor illuminated using a solar simulator. We find that $V_{bi} = 0.8$ V, indicated by the voltage where $J_{ph} = 0$, due to the difference in work functions of ITO (5.1 eV) and Ag (4.3 eV). As expected for a photoconductor, J_{ph} shows a linear dependence on applied bias and light intensity. Here $S_{pc} = 0.40 \pm 0.04$ mA/cm^2 V at a light intensity of 66 mW/cm^2 simulated AM1.5G spectrum. The response increases with light intensity, with a slope of $m = 5.7 \pm 0.2$ μA/mWV and intercept of $S_{pc,0} = 0.01 \pm 0.01$ mA/Vcm^2 as shown in the inset (Fig. 6). Measurements of an ITO/C_{60}/Ag device shows a

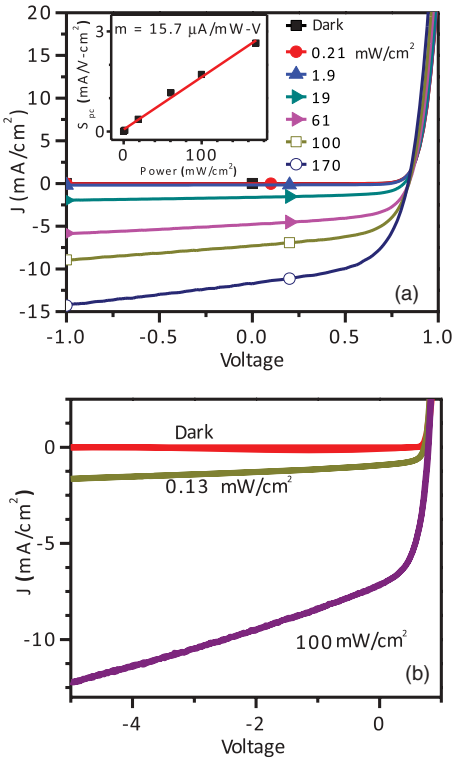

FIG. 4. (Color online) (a) Current density vs voltage (J-V) characteristics of an ITO (1500 Å)/SubPc (130 Å)/C_{60} (400 Å)/BCP (80 Å)/Ag (1000 Å) organic photovoltaic cell at various AM1.5G spectral illumination intensities from a solar simulator. The photoconductance is determined by the linear slope at reverse bias, and is plotted in the inset as a function of incident power. The fit shows a linear photoconductive response of 15.7 ± 0.6 μA/mWV. (b) The linear voltage dependence of the photocurrent shown over an extended voltage range.

similar linear response, with a $S_{pc} = 0.82 \pm 0.05$ mA/cm^{2}V at 100 mW/cm^2. We observed a weak temperature dependence of photoconductivity in the Ag/C_{60}/Ag device over the range

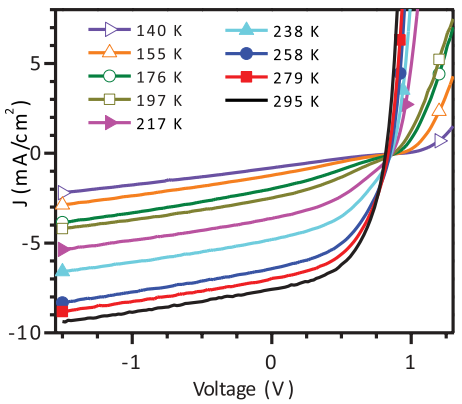

FIG. 5. (Color online) Temperature dependence of the current density vs voltage (J-V) characteristics of an ITO (1500 Å)/SubPc (130 Å)/C_{60} (400 Å)/BCP (80 Å)/Ag (1000 Å) organic photovoltaic cell. The photoconductance (S_{pc}), as apparent in the slope of the reverse biased characteristic, is almost independent of temperature, and ranges from 1.25 to 1.1 mA/Vcm^2.

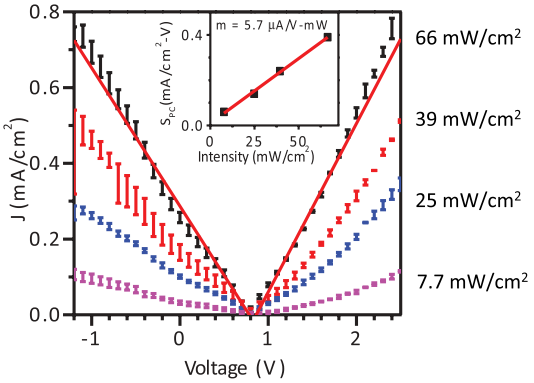

FIG. 6. (Color online) Photocurrent density vs voltage characteristics of an ITO (1500 Å)/SubPc (600 Å)/Ag (1000 Å) photoconductor measured by synchronous illumination from a solar simulator. The inset shows that the photoconductance has a linear response with incident power of 5.7 ± 0.2 μA/mW V, similar in magnitude to the photoconductive effects of the OPV devices in Fig. 5.

$140 < T < 295$ K, with an activation energy of $\Delta E_{pc} = 15 \pm 3$ meV. This behavior is similar to that of S_{pc} for the OPV, where $\Delta E_{pc} = 6.8 \pm 0.7$ meV.

V. DISCUSSION

The linear dependence of the illuminated J-V characteristics over a large reverse bias and temperature range indicates that photoconductivity plays a significant role in bilayer OPVs. In contrast, the photocurrent in excitonic BHJs often has a nonlinear reverse-biased voltage dependence,[26,27] particularly near 0 V. This suggests that field-induced dissociation of PPs, or bimolecular recombination, may dominate the photocurrent characteristics in those cases where charge trapping among the high density of bottlenecks and cul de sacs found in BHJs strongly influences transport and series resisitance.[28] In the case of bilayer HJs, however, there are large regions of homogenous composition through which excitons must diffuse to arrive at a HJ to dissociate. This provides ample opportunity for excitons to first encounter a trap site, a high energy phonon, or defect that enables bulk dissociation resulting in free-carrier generation. Hence, while we expect that photoconductivity will be less prevalent in BHJ nanomorphologies compared with bilayer planar HJs studied here, the process itself is of a fundamental origin and hence is anticipated to be present although not necessarily the dominant source of reverse-biased slope. Indeed, such a linear dependence even in polymer BHJs has been observed although it remains an open issue whether its source is of photoconductive origin.[29]

As apparent in this work, photoconductivity in bilayer HJs can potentially mask the effects of thermally activated and field-dependent PP exciton dissociation at the interface (J_{jxn}) as predicted by O-B in Eq. (1). This linear behavior begins when $V_a \approx V_{bi} - 0.5$ V, suggesting $k_{PPd} \gg k_{PPr}$ and very inefficient PP back transfer in SubPc/C_{60} heterojunctions, consistent with previous results.[30] Hence, J_{jxn} reaches a maximum (i.e., saturation) at relatively small electric fields ($\sim 10^4$–10^5 V/cm). Indeed, in Fig. 3(a) we show that in the case of $k_{PPd}/k_{PPr} \gg 1$, photoconductance can account for almost all

of the observed linearity of J under reverse bias. In Fig. 4(b) we observe that the linearity of J_{ph} extends to $V_a < -5$ V, supporting the hypothesis that photoconductivity dominates the reverse bias dependence of J_{ph}.

The temperature-dependent J-V characteristics indicate that J_{jxn} is thermally activated due to the temperature dependence of both J_x and the PP dissociation efficiency $\eta = k_{PPd.}/(k_{PPd} + k_{PPr})$. Exciton diffusion lengths have been shown to be temperature dependent[31,32]; this generates an increased J_x and a voltage independent increase in J_{ph} at high temperature. This is the dominant effect observed in Fig. 5. The temperature dependence of η is observed at $V_a > 0.5$ V, where the J-V characteristic develops an S-kink when k_{PPd} is reduced with temperature.[17] This is qualitatively similar to the reduction in current at low temperature shown in Fig. 3(a), although J_{jxn} reaches saturation at a lower reverse bias than predicted by the O-B model.

From Eq. (1), an equilibrium PP dissociation rate of $k_{PPd,eq}^{-1} = 50$ ns is obtained for $a_0 = 2$ nm. Since it is the *ratio* of $k_{PPd,eq}/k_{PPr}$ that determines J_{jxn} in Figs. 2 and 3, we infer that $k_{PPd,eq}/k_{PPr} > 10^2$ (i.e., $k_{PPr}^{-1} > 5$ μs) required for J_{jxn} to saturate and photoconductivity to dominate the voltage dependence of J_{ph} as in Fig. 3(a). Now, the PP lifetime, given by $\tau_{PP} = (k_{PPd} + k_{PPr})^{-1} \approx {k_{PPd}}^{-1}$, must be shorter than the device response time of approximately 1 ns.[33] However, $k_{PPd,eq}^{-1} = 50$ ns predicted by the O-B theory is at least 50 times *larger* than the measured device response time. To correct for this discrepancy both k_{PPd} and k_{PPr} must be scaled by the same factor to maintain the same J-V characteristics, according to Fig. 2. Hence, we infer that k_{PPr}^{-1} is > 100 ns to be consistent with the lower value of $k_{PPd,eq}^{-1}$, and hence the linearity of the reverse J-V characteristics is not explained by the PP recombination dynamics in this case.

Figure 3(b) shows the dependence of FF on $k_{PPd,eq}/k_{PPr}$ in the presence (dashed line) and absence of photoconductivity (solid line). Here FF reaches saturation for $k_{PPd,eq}/k_{PPr} > 100$, where PP back transfer or recombination across the HJ is minimal. Thus, for a physically reasonable $k_{PPd,eq}^{-1} = 1$ ns, we require that $k_{PPr}^{-1} > 100$ ns to yield a $FF > 0.7$. This value of k_{PPr} is consistent with the rate measured from the phase change observed by intensity modulated photocurrent spectroscopy of similar SubPc/C_{60} HJ OPV devices.[30] Including the contributions of photoconductance of $S_{pc} = 0.9$ mA/Vcm^2, the maximum FF obtained for a practical D-A HJ with $k_{PPd,eq}/k_{PPr} > 100$ is reduced by approximately 10% due to an increase in J_{sc} [dashed line, Fig. 3(b)]. However, the PCE of the OPV with and without the presence of photoconductivity is unchanged at the maximum power point, which is close to $V_a = V_{bi}$, where $J_{pc} \to 0$. Note, however, that the PCE can be increased due to photoconductance if the OPV is operated at voltages less than that corresponding to its value (V_m) at the *MPPT*.

The effect of photoconductance on the OPV can be understood by identifying the contributions of J_{jxn} and J_{pc} to the J-V characteristics. Using data from the photoconductor devices as in Fig. 6, we can simulate J_{pc} by first rewriting Eq. (5) as

$$\frac{J_{pc}d}{eG(V_a - V_{bi})} = \eta_{pc}(\tau_e\mu_e + \tau_h\mu_h) = \frac{S_{pc}d}{eG} \equiv \eta_{pc}\tau\mu, \quad (7)$$

where $\tau\mu = (\tau_e\mu_e + \tau_h\mu_h)$. Now, $\eta_{pc}\tau\mu$ characterizes the photoconductive sensitivity of the layers comprising the OPV. We determine $\eta_{pc}\tau\mu$ from the photoconductor device data for both the donor and acceptor, using an optical model that includes optical interference effects to calculate the local, wavelength-dependent exciton generation rate $G(x,\lambda)$[34] in the organic layers. The calculation employs the measured (by spectroscopic ellipsometry) wavelength-dependent complex refractive indicies $\tilde{n} = n + ik$. Integrating over the total active layer thickness and at all wavelengths measured, we obtain $\eta_{pc}\tau\mu = (2.2 \pm 0.3) \times 10^{-7}$ cm^2/V for SubPc, and $(4.0 \pm 0.2) \times 10^{-7}$ cm^2/V for C_{60}. We next use $\eta_{pc}\tau\mu$ to determine the carrier generation in each layer to calculate the $S_{pc} = 0.90 \pm 0.07$ mA/Vcm^2 for the OPV. Here we fit the dark current to Eq. (2) with $J_{jxn} = 0$, and obtain $J_{sA} = (1.0 \pm 0.8) \times 10^{-9}$ mA/cm^2, $J_{sD} = (4.7 \pm 1.6) \times 10^{-5}$ mA/cm^2, $R_S = 3.7 \pm 0.5$ Ωcm^2, and ideality factors of $n_A = 1.6 \pm 0.1$, and $n_D = 5.9 \pm 0.7$. These parameters, along with the calculated photoconductive response assuming $V_{bi} = 0.8$ V, then provide a simulation of the illuminated J-V data. To highlight the relative importance of J_{pc} vs J_{jxn}, in Fig. 7 we plot the experimental data (symbols) vs the calculated J-V characteristics with (solid line) and without photoconductance (dashed line) assuming $k_{PPr} \to 0$, and $J_{jxn} = qJ_X = 5.8$ mA/cm^2. Excluding photoconductance, we identify the photocurrent generated only by dissociation of PPs at the heterojunction (dashed line). By including the additional current due to photoconductivity, the simulation and the device data under illumination are in agreement over the entire range of data fit, indicating efficient PP dissociation and the importance of photoconductivity in these archetype OPV structures.

The presence of photoconductance results in an increase in J_{sc} by 15% in the SubPc/C_{60} devices. The PCE vs V is plotted in the inset of Fig. 7, and shows that photoconductivity can result in an increase in power generation over much of the fourth

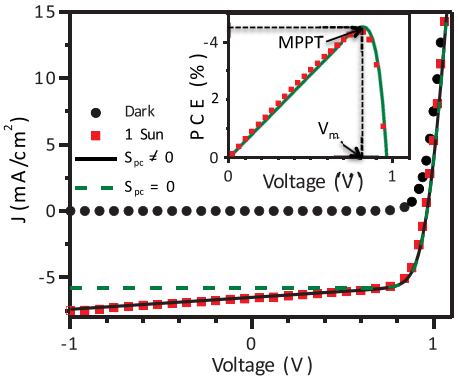

FIG. 7. (Color online) Current density vs voltage characteristic (J-V) of an ITO (1500 Å)/SubPc (130 Å)/C_{60} (400 Å)/BCP (80 Å)/Ag (1000 Å) organic photovoltaic cell in the dark (black circles) and at 1-sun intensity simulated solar illumination (red squares). Simulated current calculated using Eq. (6) (solid line) with a constant photocurrent and photoconductance of $S_{pc} = 0.9$ mA/cm^2 V for OPV. Simulated current given by Eq. (2) with a constant photocurrent and no photoconductance (green dashed line). Inset: Power conversion efficiency (PCE) under 1 sun, AM1.5G illumination vs voltage for the simulated (line) and experimental (squares) data.

quadrant of the J-V characteristic. As noted above, however, the presence of photoconductivity cannot increase the PCE $= 4.4 \pm 0.1\%$ at the *MPPT* corresponding to $V_m = 0.82 \pm 0.01$ V. The presence of photoconductivity in the active layers, however, does limit the maximum attainable fill factor to

$$FF_{\max} = 1 - (S_{pc}/J_{sc})V_{oc}, \tag{8}$$

which corresponds to $FF_{\max} = 0.79$ for a SubPc/C_{60} HJ OPV. The FF is further limited by the diode ideality [Eq. (6)] based on the ratio of $k_{PPd,eq}/k_{PPr}$, as shown in Fig. 3(b).

VI. CONCLUSIONS

In conclusion we have shown that the parallel resistance commonly observed in the J-V characteristics of organic heterojunction devices is due to exciton generation followed by dissociation in the bulk of the constituent donor and acceptor layers. Photoconductivity in the organic layers describes the observed linear increase in current under reverse bias, the temperature dependence, and the magnitude of the measured R_p. Since photoconductivity accurately describes the observed linear dependence of J_{ph} on V_a, the junction photocurrent $J_{jxn} = \eta q J_X$ is found to saturate to $q J_x$ when V_a is only a few hundred millivolts less than V_{oc}. This suggests that the polaron pair dissociation efficiency is large, indicating that $k_{PPr}^{-1} > 100\, k_{PPd,eq}^{-1}$. While photoconductance adds to the short circuit current density, it also leads to a reduced maximum fill factor, and hence imposes a constraint on the maximum power conversion efficiency when photoconductivity is significant in OPVs.

ACKNOWLEDGMENTS

This work was funded by the Center for Solar and Thermal Energy Conversion at the University of Michigan (a Department of Energy, Energy Frontier Research Center, Award No. DE-SC00000957; C.K.R., experiment and analysis, J.D.Z., device fabrication); the NSF SOLAR program (S.R.F., experimental design, analysis), and support from the collaborative R&D program with technology advanced country [2009-advanced-B-015] by the Ministry of Knowledge and Economy of Korea (B.E.L., device fabrication). We also thank Dr. L. Huang and Professor R. Krasny for numerical simulations.

[1] H. Y. Chen, J. H. Hou, X. Q. Zhang, Y. Y. Liang, G. W. Yang, Y. Yang, L. P. Yu, Y. Wu, and G. Li, Nat. Photon. **3**, 649 (2009).
[2] Y. Y. Liang, Z. Xu, J. B. Xia, S. T. Tsai, Y. Wu, G. Li, C. Ray, and L. P. Lu, Adv. Mater. **22**, E125 (2010).
[3] P. Peumans, A. Yakimov, and S. R. Forrest, J. Appl. Phys. **93**, 3693 (2003).
[4] B. P. Rand, D. P. Burk, and S. R. Forrest, Phys. Rev. B **75**, 115327 (2007).
[5] K. Schulze, C. Uhrich, R. Schuppel, K. Leo, M. Pfeiffer, E. Brier, E. Reinold, and P. Bauerle, Adv. Mater. **18**, 2872 (2006).
[6] B. T. de Villers, C. J. Tassone, S. H. Tolbert, and B. J. Schwartz, J. Phys. Chem. C **113**, 18978 (2009).
[7] P. Schilinsky, C. Waldauf, J. Hauch, and C. J. Brabec, J. Appl. Phys. **95**, 2816 (2004).
[8] Y. Lare, B. Kouskoussa, K. Benchouk, S. O. Djobo *et al.*, J. Phys. Chem. Solids **72**, 97 (2011).
[9] C. K. Renshaw, C. W. Schlenker, M. E. Thompson, and S. R. Forrest, Phys. Rev. B **84**, 045315 (2011).
[10] L. Onsager, Phys. Rev. **54**, 554 (1938).
[11] C. L. Braun, J. Chem. Phys. **80**, 4157 (1984).
[12] M. M. Mandoc, W. Veurman, L. J. A. Koster, B. de Boer, and P. W. Blom, Adv. Funct. Mater. **17**, 2167 (2007).
[13] V. I. Arkhipov, and H. Bassler, Phys. Status Solidi A **201**, 1152 (2004).
[14] R. A. Marsh, C. R. McNeill, A. Abrusci, A. R. Campbell, and R. H. Friend, Nano Lett. **8**, 1394 (2004).
[15] C. Deibel, T. Strobel, and V. Dyakonov, Adv. Mater. **22**, 4097 (2010).
[16] D. Cheyns, J. Poortmans, P. Heremans, C. Deibel, S. Verlaak, B. P. Rand, and J. Genoe, Phys. Rev. B **77**, 165332 (2008).
[17] N. C. Giebink, G. P. Wiederrecht, M. R. Wasielewski, and S. R. Forrest, Phys. Rev. B **82**, 155305 (2010).
[18] W. Jeong, Y. E. Lee, H. Shim, T. Kim, S. Kim, and J. Kim, Adv. Funct. Mater. **22**, 3089 (2012). During the preparation of this manuscript, W. Jeong *et al.*identified that photoconductivity in C_{60} contributes to the voltage-dependent photocurrent observed in planar HJ OPVs. Those results are similar to the conclusions presented here. An additional conclusion of our study is that photoconductivity can mask the field-dependent polaron pair dissociation at the HJ.
[19] P. Peumans and S. R. Forrest, Chem. Phys. Lett. **398**, 27 (2004).
[20] M. Pope and C. E. Swenberg, *Electronic Processes in Organic Crystals and Polymers* (Oxford University Press, New York, 1999).
[21] J. Day, S. Subramanian, J. E. Anthony, Z. Lu, R. J. Tweig, and O. Ostroverkhova, J. Appl. Phys. **103**, 123715 (2008).
[22] J. Reynaert, V. I. Arkhipov, P. Heremans, and J. Poortmans, Adv. Funct. Mater. **16**, 784 (2006).
[23] R. Kersting, U. Lemmer, M. Deussen, H. J. Bakker, R. F. Mahrt, H. Kurz, V. I. Arkipov, H. Bassler, and E. O. Gobel, Phys. Rev. Lett. **73**, 1440 (1994).
[24] V. I. Arkhipov, E. V. Emelianova, and H. Bassler, Phys. Rev. Lett. **82**, 1321 (1999).
[25] K. Sugiyama, H. Ishii, Y. Ouchi, and K. Seki, J. Appl. Phys. **87**, 295 (2000).
[26] M. Limpinsel, A. Wagenpfahl, M. Mingebach, C. Diebel, and V. Dyakonov, Phys. Rev. B **81**, 085203 (2010).
[27] D. Gebeyehu, B. Maennig, J. Drechsel, K. Leo, and M. Pfeiffer, Solar Energy Mater. Solar Cells **79**, 81 (2003).
[28] P. W. M. Blom, V. D. Mihailetchi, L. J. A. Koster, and D. E. Markov, Adv. Mater. **19**, 1551 (2007).
[29] V. D. Mihailetchi, H. Xie, B. de Boer, L. J. A. Koster, and P. W. M. Blom, Adv. Funct. Mater. **16**, 699 (2006).
[30] N. C. Giebink, B. E. Lassiter, G. P. Wiederrecht, M. R. Wasielewski, and S. R. Forrest, Phys. Rev. B **82**, 155306 (2010).

[31] O. V. Mikhnenko, F. Cordella, A. B. Sieval, J. C. Hummelen, P. W. M. Blom, and M. A. Loi, J. Phys. Chem. B **112**, 11601 (2008).
[32] L. S. Devi, M. K. Al-Suti, C. Dosche, M. S. Khan, R. H. Friend, and A. Kohler, Phys. Rev. B **78**, 045210 (2008).
[33] M. S. Arnold, J. D. Zimmerman, C. K. Renshaw, X. Xu, R. R. Lunt, C. M. Austin, and S. R. Forrest, Nano Lett. **9**, 3354 (2009).
[34] L. A. A. Petterson, L. S. Roman, and O. Inganas, J. Appl. Phys. **86**, 487 (1999).